

ductor lasers (3, 18) because the refractive index variation induced by the change in carrier number at the peak of the gain curve is essentially zero.

The threshold current density is determined by the condition (1, 3)

$$R \exp(\Gamma G_p - \alpha_i)L = 1 \quad (1)$$

where  $G_p = gJ_{th}$  is the peak material gain at threshold and  $\alpha_i$  is the internal loss. A good estimate for the normalized gain coefficient  $g$  was obtained experimentally from the following independent measurement: The integrated luminescence power was measured at high current density in an identical sample grown on a semi-insulating substrate to minimize losses, but without the cladding regions to eliminate gain effects, and processed in a 45° wedge configuration. The luminescence peak wavelength and linewidth were identical to that of the laser structure. From the measured luminescence power and the well-known Einstein relation between the spontaneous and stimulated emission rates,  $g$  was found to be  $9 \text{ cm}^{-1} \text{ kA}^{-1} \text{ cm}^{-2}$ . We can then recast Eq. 1 in the form

$$J_{th} = \frac{\alpha_M + \alpha_i}{g\Gamma} \quad (2)$$

where  $\alpha_M$  is the mirror loss  $-\ln(R)/L$  ( $= 18.54 \text{ cm}^{-1}$ ) and the internal loss  $\alpha_i$  (estimated to be  $\sim 9 \text{ cm}^{-1}$ ) is a combination of free carrier absorption in the graded regions and in the substrate, lateral waveguide losses, and plasmon losses in the top contact region. From Eq. 2, we obtain  $J_{th} = 6.6 \text{ kA/cm}^2$ . Considering the relatively large uncertainty in the estimation of the losses, this value is in reasonable agreement with the measured threshold. We were able to operate a few devices at temperatures as high as 88 K with comparable thresholds and clear evidence of spectral narrowing. Improved device processing and heat sinking will allow a systematic study at this and higher temperatures. Preliminary evidence shows that, as expected, the temperature dependence of the threshold current density is much weaker than that in diode lasers (3).

## REFERENCES AND NOTES

1. See, for example, A. Yariv, *Quantum Electronics* (Wiley, New York, 1988), chap. 10.
2. R. N. Hall, G. E. Fenner, J. D. Kingsley, T. J. Soltys, R. O. Carlson, *Phys. Rev. Lett.* **9**, 366 (1962); M. I. Nathan, W. P. Dumke, G. Burns, F. H. Dill Jr., G. Lasher, *Appl. Phys. Lett.* **1**, 62 (1962); T. M. Quist *et al.*, *ibid.*, p. 91; N. J. Holonyak and S. F. Bevacqua, *ibid.*, p. 82. The modern double-heterostructure injection laser was demonstrated by H. Kressel and H. Nelson [*ACA Rev.* **30**, 106 (1969)], Zh. Alferov, V. M. Andrej, E. L. Portnoi, and M. K. Trukan [*Sov. Phys. Semicond.* **3**, 1107 (1970)], and I. Hayashi, M. B. Panish, P. W. Foy, and S. Sumski [*Appl. Phys. Lett.* **17**, 109 (1970)]. Its concept was proposed by H. Kroemer [*Proc. IEEE* **51**, 1782 (1963)].
3. For a recent review of semiconductor lasers, see G. P. Agrawal and N. K. Dutta, *Long-Wavelength*

*Semiconductor Lasers* (Van Nostrand Reinhold, New York, 1986).

4. This holds true also for quantum well lasers, where the band gap of the well material is effectively increased by the quantum confinement of electrons and holes.
5. A. Y. Cho, *J. Cryst. Growth* **111**, 1 (1991).
6. F. Capasso, *Science* **235**, 172 (1987).
7. R. F. Kazarinov and R. A. Suris, *Sov. Phys. Semicond.* **5**, 207 (1971); for a detailed discussion of this and similar schemes, see F. Capasso, K. Mohammed, A. Y. Cho, *IEEE J. Quantum Electron.* **22**, 1853 (1986). For more recent proposals, see A. Kastalsky, V. J. Goldman, J. Abeles, *Appl. Phys. Lett.* **59**, 2636 (1991); J. P. Lohr, J. Singh, R. K. Mains, G. I. Haddad, *ibid.*, p. 2070; S. I. Borenstein and J. Katz, *ibid.* **55**, 654 (1989).
8. L. Esaki and R. Tsu, *IBM J. Res. Dev.* **14**, 61 (1970).
9. Before the invention of the diode laser, a semiconductor laser based on transitions between Landau subbands in a magnetic field was proposed by B. Lax [in *Proceedings of the International Symposium on Quantum Electronics*, C. H. Townes, Ed. (Columbia Univ. Press, New York, 1960), p. 428]. During the last decade, lasers based on infrared emission by hot holes in crossed electric and magnetic fields in *p*-type Ge have been demonstrated. These sources, based on various mechanisms, including cyclotron emission, are of limited technological interest. For a review, see A. A. Andronov, *Sov. Phys. Semicond.* **21**, 701 (1987).
10. The electronic states of our  $\text{Al}_{0.48}\text{In}_{0.52}\text{As}-\text{Ga}_{0.47}\text{In}_{0.53}\text{As}$  coupled-well structure (Fig. 1A) were calculated in the envelope function approximation for various electric fields. The material parameters were conduction band discontinuity  $\Delta E_c = 0.52 \text{ eV}$ , electron effective mass  $m_e^*(\text{GaInAs}) = 0.043 m_0$ , where  $m_0$  is the free electron mass, and  $m_e^*(\text{AlInAs}) = 0.078 m_0$ . For the nonparabolicity coefficient, we used  $\gamma = 1.13 \times 10^{-18} \text{ m}^2$ . Nonparabolicities were taken into account with the method of D. F. Nelson, R. C. Miller and D. A. Kleinman [*Phys. Rev. B* **35**, 7770 (1987)].
11. Narrow ( $\sim 1 \text{ meV}$ ) lifetime-broadened Lorentzian intersubband transitions at energies  $\sim 140 \text{ meV}$ , with high oscillator strengths, have recently been observed in absorption in high-quality selectively doped  $\text{AlGaAs}-\text{GaAs}$  coupled quantum wells. See J. Faist, C. Sirtori, F. Capasso, L. Pfeiffer, K. West, *Appl. Phys. Lett.* **64**, 872 (1994).
12. F. Capasso, H. M. Cox, A. L. Hutchinson, N. A. Olsson, S. G. Hummel, *Appl. Phys. Lett.* **45**, 1193 (1984).
13. F. Capasso, W. T. Tsang, G. F. Williams, *IEEE Trans. Electron Devices* **30**, 381 (1983).
14. P. J. Price, *Ann. Phys.* **133**, 217 (1981).
15. J. Faist *et al.*, unpublished results.
16. J. Faist *et al.*, *Appl. Phys. Lett.* **64**, 1144 (1994).
17. A. L. Schawlow and C. H. Townes, *Phys. Rev.* **112**, 1940 (1958).
18. C. H. Henry, *IEEE J. Quantum Electron.* **19**, 1391 (1983).
19. We thank R. F. Kazarinov, S. Luryi, and D. V. Lang for comments and discussions.

14 February 1994; accepted 28 February 1994

## A Mechanism of Lithium Storage in Disordered Carbons

Kenji Sato,\* Minoru Noguchi, Atsushi Demachi, Naohiko Oki, Morinobu Endo

High-resolution electron microscopy and lithium-7 nuclear magnetic resonance measurements were carried out for a disordered carbon material, prepared by heat treatment of polyphenylene, in which lithium was stored electrochemically. The nuclear magnetic resonance spectrum suggests the existence of  $\text{Li}_2$  covalent molecules in the carbon material. This extra covalent site of lithium storage promises extraordinarily high energy density for secondary batteries.

Graphite can store various kinds of species, such as potassium and bromine, between the crystalline sheets to form stage compounds called graphite intercalation compounds (GICs) (1). Under certain conditions, graphite stores Li ions electrochemically, forming a GIC. The storage process is reversible, so that graphite can be used instead of metallic Li as the negative electrode in Li secondary batteries (2). Various kinds of graphite and carbons have been studied as candidates for the negative electrode material of so-called Li ion batteries (2, 3). The Li ion batteries are expected to lead to weight elimination for portable electronics apparatus such as video cameras and lap-top

personal computers. Advantages include their high electromotive force of around 3 to 4 V; their high energy density, higher than that of any conventional secondary batteries; and their safety, as no metallic Li is used. Recently, some disordered carbons were shown to have a specific capacity much higher than that expected from the first-stage GIC stoichiometry ( $\text{C}_6\text{Li}$ , 372 A·hour/kg) (3, 4), where the Li is inserted at maximum density between each graphite sheet. These extremely high capacities suggest that there may be a mechanism different from the common well-staged compounds of graphite.

We have synthesized a disordered carbon material that stores Li with a mechanism completely different from that in GICs. High-resolution electron microscopy images as well as  $^7\text{Li}$  nuclear magnetic resonance (NMR) spectroscopic evidence indicate a Li storage mechanism by an electrochemical process. This phenomenon

K. Sato, M. Noguchi, A. Demachi, N. Oki, Honda Research and Development Co., Ltd., Wako Research Center, 1-4-1 Chuo, Wako-shi, Saitama, 351-01 Japan. M. Endo, Faculty of Engineering, Shinshu University, 500 Wakasato, Nagano, 380 Japan.

\*To whom correspondence should be addressed.

could provide a promising development for high-energy Li battery applications.

Poly(*p*-phenylene) (PPP) was synthesized by the Kovacic method (5). The PPP thus synthesized had structural irregularities such as branching, bending, and cross-linking. It was heat-treated under hydrogen flow at 973 K, and the PPP-based carbon thus obtained had a largely disordered structure, so that x-ray diffraction showed no clear (002) reflections (3). Elemental analysis of the sample gave an H/C ratio of 0.24.

Electrodes made of the PPP-based carbon were charged and discharged at a current density of 1.6 mA/cm<sup>2</sup>. This current density is an order of magnitude higher than those applied to electrodes made of highly crystallized graphite. The PPP-based carbon is suitable for high-power battery applications. Excellent reversibility and specific discharge capacity of 680 A·hour/kg, which exceeds the first-stage GIC stoichiometry, was observed. Because the electrochemical potential of Li-doped PPP-based carbon is higher than that of Li-doped graphite at the same depth of doping, the electromotive force of a Li ion battery made with PPP-based carbon will be lower than that made with graphite.

Lattice images of high-resolution transmission electron microscopy on pristine PPP-based carbon (Fig. 1A) and Li-charged PPP-based carbon (which forms C<sub>6</sub>Li) (372 A·hour/kg) (Fig. 1B) do not show the stacked layer structure that is characteristic of crystalline graphite. Characteristic defective structure is clearly seen where short graphite sheets are randomly located. It is difficult to characterize these samples by an interlayer spacing as determined from an (002) x-ray diffraction peak because these samples have no clear (002) peak, as in conventional carbons and graphites, corresponding to the interlayer spacing of about 3.440 to 3.354 Å. From these images, it is evident that Li doping creates a much more defective lattice of PPP-based carbon as compared with the disordered structure before Li doping. The interlayer spacing is estimated to increase by about 10% to ~4.0 Å in pristine PPP-based carbon, as determined from the fast Fourier transform (FFT) patterns (6) corresponding to Fig. 1. This suggests that the Li ions are located among the defective carbon layers. This expansion of the layer spacing is similar to that of well-ordered graphite, where the interlayer spacing increases by about 10% during Li intercalation to form C<sub>6</sub>Li (7).

The <sup>7</sup>Li NMR spectrum of Li-doped PPP-based carbon (Fig. 2A) reveals no metallic bands, and a main band with fine structure is clearly observed around 0 ppm, accompanied by spinning side bands. Superposition of the three bands A, B, and C can well reproduce the observed line shape

of the main band (Fig. 2B). The Li doped in PPP-based carbon must occupy two different sites corresponding to bands A and B. Band C can be assigned to the by-product lithium carbonate, which is detected by electron spectroscopy for chemical analysis and by infrared spectroscopy, and is not essential in the following discussion. Band A has a Gaussian line shape (characteristic feature of a solid phase) with a chemical shift of 9.85 ppm and a half width of 11.6 ppm. Band B has, in contrast, a Lorentzian line shape (characteristic feature of a liquid or gas phase) with a chemical shift of -0.62 ppm and a half width of 8.9 ppm. Band B has been observed in differently doped levels from 30 to 1000 A·hour/kg, and the chemical shift lies within ±1.0 ppm. Band A is observed when the specific charge capacity is more than 300 A·hour/kg, and the chemical shift value increases with greater Li doping.

The nature of band A can be understood from the doping of a Li ion into PPP-based carbon, which is accompanied by electron occupation in the lowest unoccupied molecular orbital (LUMO) of PPP-based carbon and gives rise to radical formation. The <sup>7</sup>Li nuclear spin may be coupled with the electronic spin of the radical. The NMR chemical shift of a radical is proportional to the electronic

spin density at the position of the observed nucleus (8). The finite chemical shift for site A suggests that electronic spin density has a finite value at the position of the <sup>7</sup>Li nucleus. This mechanism is analogous to that in GICs (correctly speaking in the case of crystalline graphite hosts, the electronic spin is produced by a Pauli paramagnetism mechanism caused by the applied magnetic field). The Gaussian line shape of band A is consistent with the ionic mechanism, where <sup>7</sup>Li nuclei are fixed and inhomogeneous broadening determines the line shape. Namely, site A can be considered as an ionic or GIC site.

Band B may be caused by the existence of molecular Li<sub>2</sub> in the PPP-based carbon. In a Li<sub>2</sub> molecule, all electrons form pairs and the total electronic spin is zero. Therefore, the

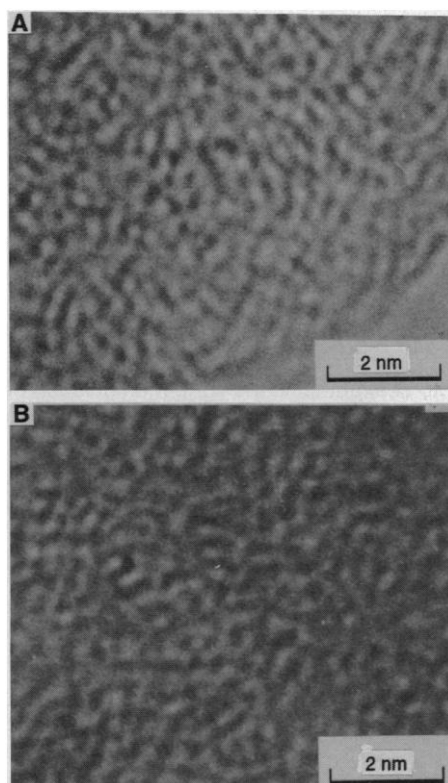


**Fig. 1.** High-resolution lattice images, obtained by transmission electron microscopy at a 400-kV acceleration voltage, of (A) pristine and (B) Li-doped (C<sub>6</sub>Li) PPP-based carbon. The defective structure is clearly seen.

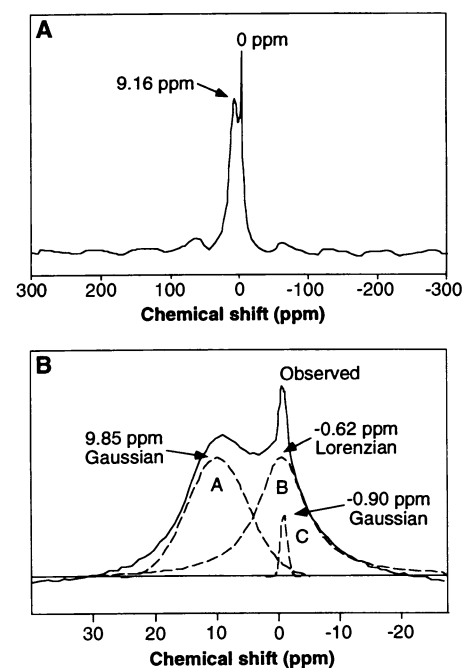
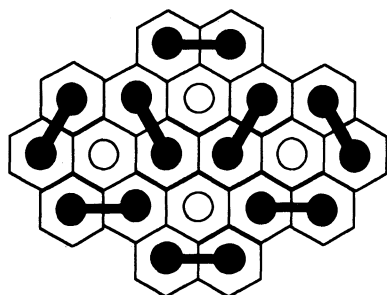


**Fig. 2.** (A) Nuclear magnetic resonance spectra of <sup>7</sup>Li in heat-treated PPP for a specific charge capacity of 1000 A·hour/kg. (B) Nuclear magnetic resonance line shape simulation for the main band around 0 parts per million in (A). A mixture of heat-treated PPP and polyethylene binder was pressed into a pellet. A three-electrode electrochemical cell was assembled with the pellet as a working electrode and lithium foil as counter and reference electrodes. A solution of 1 mol of lithium hexafluorophosphate per liter of a mixture of propylene carbonate and dimethoxy ethane (volume ratio, 1/1) was used as an electrolyte. The current density was 1.6 mA/cm<sup>2</sup>. Sample preparation was done under dry argon atmosphere. The charged electrode was rinsed with dimethoxy ethane to remove electrolyte, dried, mixed with KBr powder, and put into a solid NMR sample tube. Measurements were carried out on a magic angle spinning NMR spectrometer (Nihon Denshi Co., Ltd., Tokyo) with a field strength of 6.3 T (105 MHz for <sup>7</sup>Li). A standard material was 1 M LiCl. Line shape simulation was performed with a computer program developed by Nihon Denshi.

electron-nuclear spin interaction does not exist. A very small chemical shift for band B is consistent with a  $\text{Li}_2$  molecule model. This model is also consistent with a Lorentzian line shape. The intermolecular force between two  $\text{Li}_2$  molecules is based on a weak van der Waals bond, and  $\text{Li}_2$  molecules can move rather freely. Therefore, the magnetic effect caused by surrounding nuclei is averaged in the same way as in a liquid phase. In a liquid phase, the NMR line shape is determined by the relaxation through spin-spin interaction. The observed half width for band B is not much narrower than that of band A. We suppose that there is a very efficient spin-spin relaxation process in a  $\text{Li}_2$  molecule mediated by bonding electrons. Site B may be called a "covalent" site.

The extra specific capacity of PPP-based carbon can be interpreted to result from the presence of the "covalent" site B. The capacity of site A may be restricted by the GIC stoichiometry, whereas the capacity of site B may have no limit opposed by the electronic system stability because occupation of site B involves little change in the electronic state of the carbon host. Only a geometrical limit exists for the B site capacity. The most saturated state may be  $\text{C}_2\text{Li}$ , where each benzene ring of PPP-based carbon is accompanied by one Li atom.

The charge-discharge mechanism of the lithium ion in PPP-based carbon can be understood as follows (Fig. 3). The Li ions in site A form a  $\sqrt{3} \times \sqrt{3}$  commensurate lattice structure, which is the reason for the stoichiometric restriction of site A, similar to that in the well-known Li GIC (1). A  $\text{Li}_2$  molecule in covalent site B is loosely trapped upon two adjacent benzene rings, which are not occupied by site A Li ions. The bond



○ Site A Li (ionic)  
● Site B Li (covalent)

**Fig. 3.** Schematic illustration for the coexistence of two types of Li site in PPP-based carbon. Reduced aromatic rings are represented by hexagonals. The Li ions and atoms are denoted by empty and solid circles for sites A and B, respectively. Covalent bonds between two Li atoms in site B are shown by heavy lines.

length of  $\text{Li}_2$  is 2.672 Å (9), which is slightly longer than the distance between the centers of two adjacent hexagonal rings (2.46 Å). Therefore, Fig. 3 is not a geometrically unacceptable image. The distance between two nearest neighbor Li atoms in metallic Li is 3.032 Å. Only a covalent character in the Li-Li bond can make the occupation of site B possible. In the charging process, site B is occupied at first, and then, after the charged capacity has exceeded 300 A·hour/kg, site A occupation begins. In the discharging process, Li ions in ionic A sites are released at first. When a vacancy on site A is created, it is reoccupied through dissociation and charge transfer reaction of  $\text{Li}_2$  molecules on B sites. The  $\text{Li}_2$  molecules in B sites are able to act as a capacity reservoir.

Assuming that each benzene ring of PPP-based carbon can supply one site for Li occupation, the calculated specific capacities per weight and per volume are 1157 A·hour/kg and 2983 A·hour/liter, respectively. Those for Li metal are 3862 A·hour/kg and 2061 A·hour/liter, respectively. These high specific capacities suggest the possibility of a high-energy battery that is more compact when made with Li ions (or molecules) than when made with Li metal.

Recently, Conard *et al.* (10) synthesized highly saturated Li GIC ( $\text{C}_2\text{Li}$ , 1116 A·hour/kg) from highly oriented pyrolytic

graphite under high pressure (50 to 60 kbar). The PPP-based carbon can store almost the same amount of Li under ambient pressure and temperature by an electrochemical reaction on a nanometer length scale in disordered carbons. This phenomenon may provide a promising breakthrough and future for high-energy Li batteries to be used for various applications.

## REFERENCES AND NOTES

1. M. S. Dresselhaus and G. Dresselhaus, *Adv. Phys.* **30**, 139 (1981).
2. T. Nagaura and T. Tozawa, *Prog. Batteries Sol. Cells* **9**, 209 (1990).
3. M. Noguchi, K. Miyashita, M. Endo, *Tanso* **155**, 315 (1992).
4. S. Yata *et al.*, in *Proceedings of the 60th Conference of the Electrochemical Society of Japan*, T. Nonaka, Ed. (Electrochemical Society of Japan, Tokyo, 1993), p. 184.
5. P. Kovacic and A. Kyriakis, *J. Am. Chem. Soc.* **85**, 454 (1963).
6. K. Oshida *et al.*, *J. Mater. Res.* **8**, 512 (1993).
7. D. Guerard and A. Herold, *Carbon* **13**, 337 (1975).
8. A. Abragam, *The Principles of Nuclear Magnetism* (Oxford Univ. Press, Oxford, 1961), pp. 191-210.
9. F. W. Loomis and R. E. Nussbaum, *Phys. Rev.* **38**, 1447 (1931).
10. J. Conard, V. A. Nalimova, D. Guerard, in *Extended Abstracts of the 7th International Symposium on Intercalation Compounds*, J. P. Issi, Ed. (Organizing Committee of ISIC7, Louvain-La Neuve, 1993), p. 114.

3 November 1993; accepted 1 March 1994

## A Putative Role of the Xanthophyll, Zeaxanthin, in Blue Light Photoreception of Corn Coleoptiles

Miguel A. Quiñones\* and Eduardo Zeiger†

Both flavins and carotenoids have some of the attributes expected for a photoreceptor mediating blue light-induced phototropism in plants. Besides the classical photoreceptor candidate,  $\beta$ -carotene, coleoptiles contain many other carotenoids, including the main components of the xanthophyll cycle, violaxanthin and zeaxanthin. Here, dark-grown coleoptiles accumulated violaxanthin, but lacked zeaxanthin. Coleoptiles devoid of zeaxanthin did not bend in response to a blue light pulse. Coleoptile tips converted violaxanthin into zeaxanthin in the light. Manipulation of coleoptile zeaxanthin content by red light, red light plus darkness, or incubation with the inhibitor of zeaxanthin formation, dithiothreitol, resulted in a blue light-induced bending that was proportional to zeaxanthin content. These data indicate that zeaxanthin may be a blue light photoreceptor in corn coleoptiles.

The identity of the photoreceptor for blue light-induced phototropism (1) remains unknown. Available action spectra (2) implicate both flavins and carotenoids, and a plasma membrane-bound flavoprotein is currently hypothesized as the most likely chromophore (3). On the other hand, chloroplasts may be

a site of photoreception for phototropism in oat coleoptiles (4), and guard cell chloroplasts show a blue light response that has an action spectrum matching the absorption spectrum of carotenoids (5). Here, we investigated whether the carotenoid, zeaxanthin, which has an absorption spectrum matching the action spectrum for phototropism (2), could mediate blue light-induced phototropic bending. In chloroplasts from higher plants, violaxanthin is converted to zeaxanthin in the light by way of an intermediate, antheraxanthin (6). Zeaxanthin reverts to violaxanthin

Department of Biology, University of California at Los Angeles, Los Angeles, CA 90024, USA.

\*Present address: Centro de Investigaciones Biológicas-Consejo Superior de Investigaciones Científicas, Velázquez 144, Madrid-28006, Spain.

†To whom correspondence should be addressed.